Implementation of a two-stroke quantum heat engine with a collisional model

Filipe V. Melo, Nahum Sá ⬤, Itzhak Roditi ⬤, Alexandre M. Souza, Ivan S. Oliveira, and Roberto S. Sarthour
Centro Brasileiro de Pesquisas Físicas, 22290-180 Rio de Janeiro, Rio de Janeiro, Brazil

Gabriel T. Landi
Instituto de Física da Universidade de São Paulo, 05508-090 São Paulo, Brazil
School of Physics, Trinity College Dublin, College Green, Dublin 2, Dublin D02 PN40, Ireland

We put forth a quantum simulation of a stroboscopic two-stroke thermal engine in the IBM quantum (IBMQ) processor. The system consists of a quantum spin chain connected to two baths at their boundaries, prepared at different temperatures using the variational quantum thermalizer algorithm. The dynamics alternates between heat and work strokes, which can be separately designed using independent quantum circuits. The results show good agreement with theoretical predictions, showcasing IBMQ as a powerful tool to study thermodynamics in the quantum regime, as well as the implementation of variational quantum algorithms in real-world quantum computers. It also opens the possibility of simulating quantum heat transport across a broad range of chain geometries and interactions.

I. INTRODUCTION

Energetics of quantum devices is an active topic of research [1], with many unique features. Quantum chains may present anomalous heat transport [2,3], negative differential conductivity [4], and perfect rectification [5]. Often, the interaction energy between two systems is comparable to that of their individual parts [6–9], causing the local notion of energy as belonging to individual systems to break down. As a consequence, the separation between heat and work may become nontrivial especially in the presence of quantum coherence. In the quantum domain, other resources also come into play: Quantum correlations, for example, can be consumed to make heat flow from cold to hot [10–12], similar to how electric energy is consumed to run a fridge. Finally, the invasive nature of quantum measurements makes all the above quantities extrinsic to the specific choice of measurement protocol [13–16].

The above arguments highlight the need for further experiments, able to assess the energetics of specific quantum devices. In this respect, quantum heat engines [17,18] are particularly interesting, as they epitomize the fundamental questions of the field. Several experimental demonstrations of quantum heat engines have been put forth in recent years, including in trapped ions [19–22], single electron boxes [23,24], superconducting devices on the IBM quantum (IBMQ) network [25,26], nuclear magnetic resonance [27,28], silicon tunnel field-effect transistor [29], electromagnetically induced transparency [30], and nitrogen vacancy centers [31,32].

In this paper we provide a demonstration of a quantum simulation of a stroboscopic, two-stroke quantum heat engine in the IBM quantum processor [33], based on a collisional model. We focus on two-stroke engines, which alternate between heat and work strokes in a generalization of the so-called SWAP engines [34–40]. The working fluid is a one-dimensional quantum chain with both ends connected to thermal baths at different temperatures. Implementing thermal baths in quantum processors is notoriously difficult. In our setup this is overcome using a variational quantum thermalizer algorithm as put forth by Verdon *et al.* in Ref. [41] and detailed further below. For the heat strokes, the sites are uncoupled from each other and allowed to interact with the baths at the boundaries. Conversely, in the work stroke the baths are uncoupled, and the qubits are allowed to interact with their nearest neighbors according to an arbitrary interaction [40]. The demonstrations are performed in the engine, refrigerator, and accelerator configurations. We study both the transient dynamics as well as the limit cycle. Our framework shows a procedure to implement quantum heat engines in a cloud quantum computing platform, providing a way to prepare the thermal baths through the variational quantum thermalizer algorithm and showing that it is possible to implement a collisional model with a single qubit using reset operations when the system-bath interaction time is short enough. With the increasing availability of cloud quantum computing services, the elaboration of methods to study quantum thermal machines in those devices is quite relevant.

The paper is organized as follows: Section II provides a theoretical background for the quantum heat engine provided. The quantum simulation setup is described in Sec. III, and the results are discussed in Sec. IV.

II. TWO-STROKE QUANTUM HEAT ENGINE

The basic idea is depicted in Sec. II. Our design, shown in Fig. 1(b), involves two separate and independent circuit implementations for the heat and work strokes. This has the
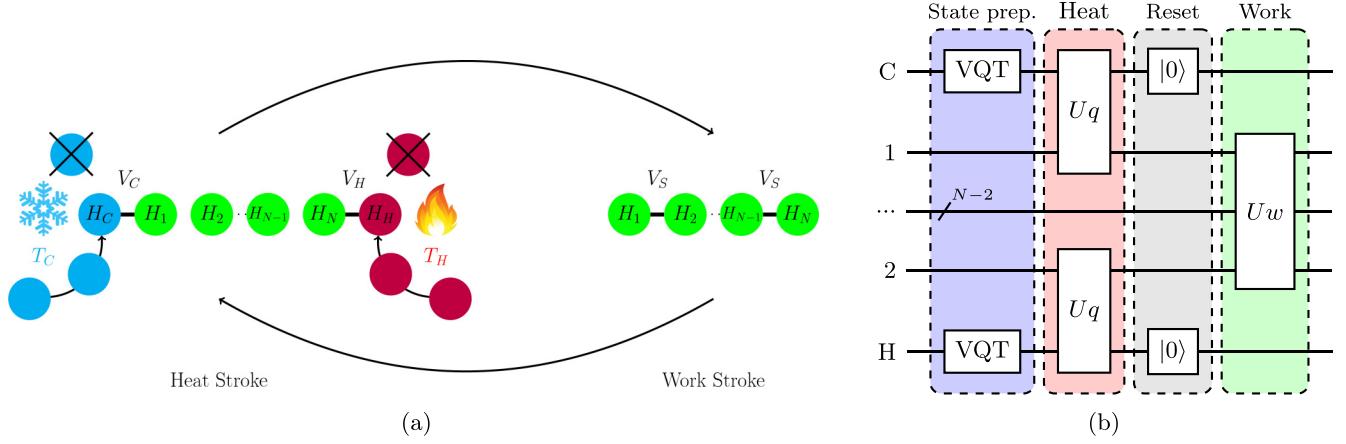
FIG. 1. The quantum heat engine operates in two modes as shown in (a): the heat stroke and the work stroke. In the heat stroke, the internal interactions of the quantum chain are turned off, and the system boundary qubits interact with a cold bath at temperature T_C and a hot bath at temperature T_H both described by auxiliary qubits. In the work stroke, the baths are uncoupled, and the chain qubits interact with their nearest neighbors. The strokes are operated in a cyclic way, and before each heat stroke the auxiliary qubits are discarded and new ones are introduced, according to the collisional model. The one-cycle circuit configuration, shown in (b), consists of $N + 2$ qubits (in our case $N = 2$). At the beginning, bath qubits C and H in the $|0\rangle$ state are processed with the circuit found with the variational quantum thermalizer (VQT) algorithm to prepare them in thermal states at temperatures T_C and T_H. A set of gates implement the heat stroke via a unitary U_q when qubits 1 and N are measured. The procedure is repeated until the work stroke, which is implemented via an unitary U_w, after which all the qubits in the chain are measured. The auxiliary qubits are reset to $|0\rangle$ for the next cycle.

unique advantage that it holds for any internal interaction during the work stroke. As a consequence, it can be implemented for any chain size and interaction that is programmable on the simulator.

The two-stroke heat engine we implement consists of a quantum chain with N-uncoupled qubits, each with local Hamiltonian H_i and prepared in an arbitrary global state ρ_S. The qubits can interact with their nearest neighbors with a Hamiltonian $V_s = \sum_i V_{i,i+1}$ that can be turned on and off. In addition, one can also turn on and off an interaction between the qubits at the boundaries and two heat baths, modeled by identical and independently prepared qubits with Hamiltonians H_x and prepared in thermal states $\rho_x = e^{-H_x/T_x}/Z_x$ with $x \in \{C, H\}$, being C for cold and H for hot, Z_x is the partition function, and $T_C < T_H$ (we set $k_B = 1$).

The dynamics alternate between heat and work strokes. During the heat stroke, the internal interactions are turned off, whereas the boundary qubits interact with their respective baths C and H via Hamiltonians V_C and V_H. The system, thus, evolves for a period τ_q, under the action of a Hamiltonian, $H_q = \sum_i H_i + H_C + H_H + V_C + V_H$ and with an evolution characterized by the map,

$$\tilde{\rho}_S = \mathcal{E}_q(\rho_S) = \mathrm{Tr}_{CH}\{U_q(\rho_C \rho_S \rho_H)U_q^{\dagger}\}, \qquad (1)$$

where $U_q = e^{-iH_q\tau_q}$. In the work stroke, the baths are disconnected from the chain, and the internal interactions V_S are turned on, allowing energy to flow through the chain. The system evolves for a time τ_w under the action of the Hamiltonian $H_w = \sum_i H_i + V_S$, according to the map,

$$\rho_S' = \mathcal{E}_w(\rho_S) = U_w \tilde{\rho}_S U_w^{\dagger}, \qquad (2)$$

where $U_w = e^{-iH_w\tau_w}$. The execution of the two strokes in succession results in a cycle of duration $\tau = \tau_q + \tau_w$. Figure 1(b) illustrates one such cycle. Crucially, for each new cycle the

baths C and H are reset to the same temperatures T_C and T_H as in a collisional model [42]. The machine, thus, follows a stroboscopic dynamics. Letting ρ_S^n denote the initial state of the nth cycle, and $\tilde{\rho}_S^n$ is the intermediate state between the strokes, the dynamics is given by

$$\tilde{\rho}_S^n = \mathcal{E}_q(\rho_S^n), \qquad \rho_S^{n+1} = \mathcal{E}_w(\tilde{\rho}_S^n). \qquad (3)$$

By splitting the dynamics in two strokes, we have reduced the problem to two independent simulation designs. For the work stroke, one need only to design U_w. Conversely, for the heat stroke, one must design both U_q and the thermal states of the baths. The implementation of the latter is, in practice, quite difficult and is overcome here using the variational quantum thermalizer algorithm [41] as explained in Sec. III D.

In order to track the energetics of the engine, we can measure the energy changes in the baths and the system during each cycle. In the heat stroke of the nth cycle, we define heat as the change in energy of the baths,

$$Q_x^n = -\mathrm{Tr}\left\{H_x(\tilde{\rho}_x^n - \rho_x)\right\}, \qquad (4)$$

which are positive when energy enters the system. Note that ρ_x is the same for all cycles since the baths are reset. The heat Q_x^n is, in general, different from the change in energy of the system, as there may be a work cost associated with turning on/off the interactions $V_{C(H)}$. From global energy conservation, we find that [42],

$$W_C^{\mathrm{on/off}} = Q_C^n + \mathrm{Tr}\left\{H_1(\tilde{\rho}_S^n - \rho_S^n)\right\} = -\Delta V_C^n,$$
$$W_H^{\mathrm{on/off}} = Q_H^n + \mathrm{Tr}\left\{H_N(\tilde{\rho}_S^n - \rho_S^n)\right\} = -\Delta V_H^n, \qquad (5)$$

with $\Delta V_x^n = \mathrm{Tr}\{V_x(\tilde{\rho}_{CSH}^n - \rho_C \rho_S^n \rho_H)\}$.

This work term only vanishes when

$$[V_C, H_1 + H_C] = [V_H, H_N + H_H] = 0, \qquad (6)$$

a condition known as *strict energy conservation* [40]. When this is satisfied, we can write

$$Q_C^n = \text{Tr}\left\{H_1\left(\tilde{\rho}_S^n - \rho_S^n\right)\right\}, \quad Q_H^n = \text{Tr}\left\{H_N\left(\tilde{\rho}_S^n - \rho_S^n\right)\right\}, \quad (7)$$

meaning that all energy that leaves the bath enters the system and vice versa. Thus, one can determine the change in energy during the heat stroke measuring only the state of the system chain.

During the work stroke, the interactions $V_S = \sum_i V_{i,i+1}$ are turned on so that energy is allowed to flow through the chain. The work cost associated with this is now connected to turning V_S on and off,

$$W^n = -\text{Tr}\left\{\left(\sum_i H_i\right)\left(\rho_S^{n+1} - \tilde{\rho}_S^n\right)\right\} = \text{Tr}\left\{V_S\left(\rho_S^{n+1} - \tilde{\rho}_S^n\right)\right\}, \quad (8)$$

which is defined as positive when energy leaves the system.

After several strokes, the engine will reach a limit cycle such that,

$$\tilde{\rho}_S^* = \mathcal{E}_q(\rho_S^*), \quad \rho_S^* = \mathcal{E}_w(\tilde{\rho}_S^*). \quad (9)$$

The system, therefore, alternates between $\tilde{\rho}_S^*$ and ρ_S^* after each stroke, and Eqs. (7) and (8) become

$$Q_C^* = \text{Tr}\left\{H_1(\tilde{\rho}_S^* - \rho_S^*)\right\}, \quad (10)$$

$$Q_H^* = \text{Tr}\left\{H_N(\tilde{\rho}_S^* - \rho_S^*)\right\}, \quad (11)$$

$$W^* = -\text{Tr}\left\{\left(\sum_i H_i\right)(\rho_S^* - \tilde{\rho}_S^*)\right\}. \quad (12)$$

At the limit cycle, the system internal energy no longer changes so that

$$Q_C^* + Q_H^* = W^*, \quad (13)$$

which is the first law.

III. IMPLEMENTATION SETUP

In this paper, we present an implementation of the just-described engine in IBM_LAGOS (v1.0.8), which is one of the IBM quantum Falcon processors, based on superconducting qubits [43]. The use of this quantum processor is accessible through the cloud along with other similar devices in Ref. [33] and can be remotely controlled via a personal computer with the open-source PYTHON framework QISKIT [44], also offered by IBM.

A. System configuration

The system consists of a chain of $N = 2$ nonresonant qubits ($\omega_1 \neq \omega_2$) with Hamiltonians,

$$H_1 = \frac{\omega_1}{2}\sigma_z^1, \quad H_2 = \frac{\omega_2}{2}\sigma_z^2, \quad (14)$$

and two ancillary qubits to represent the thermal baths,

$$H_C = \frac{\omega_C}{2}\sigma_z^C, \quad H_H = \frac{\omega_H}{2}\sigma_z^H. \quad (15)$$

All the interactions are chosen to be of the form

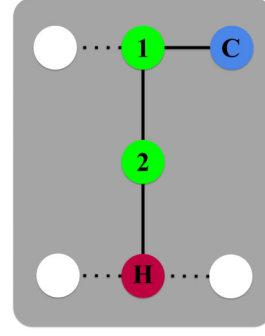$$V_{j,k} = g_{j,k}(\sigma_+^j\sigma_-^k + \sigma_-^j\sigma_+^k), \quad (16)$$

FIG. 2. The picture represents the topology of the quantum chip IBM_LAGOS. Nodes and edges represent qubits and their connections, respectively. Nodes 1 and 2 represent the quantum chain with two qubits. Nodes C and H represent the auxiliary qubits that are used as the cold and hot baths, respectively. Unlabeled nodes and dashed edges are qubits and connections that were not used.

where $\sigma_\pm = \sigma_x \pm i\sigma_y$. This concerns the heat stroke interactions $V_C = V_{1,C}$ and $V_H = V_{2,H}$, as well as the work stroke interaction $V_{1,2}$. The baths are assumed to be resonant with their sites ($\omega_C = \omega_1$ and $\omega_H = \omega_2$) from which one finds that Eq. (16) satisfies the conditions (6).

From Eq. (7), the heats for the nth cycle are given by

$$Q_C^n = \frac{\omega_1}{2}\left(\langle\tilde{\sigma}_z^1\rangle_n - \langle\sigma_z^1\rangle_n\right), \quad Q_H^n = \frac{\omega_2}{2}\left(\langle\tilde{\sigma}_z^2\rangle_n - \langle\sigma_z^2\rangle_n\right), \quad (17)$$

where $\langle\sigma_z^i\rangle_n = \text{Tr}\{\sigma_z^i\rho_S^n\}$ and $\langle\tilde{\sigma}_z^i\rangle_n = \text{Tr}\{\sigma_z^i\tilde{\rho}_S^n\}$. Following Eq. (8), the work for the nth cycle is

$$W^n = -\sum_{i=1,2}\frac{\omega_i}{2}\left(\langle\sigma_z^i\rangle_{n+1} - \langle\tilde{\sigma}_z^i\rangle_n\right). \quad (18)$$

B. Hardware

The topology of the seven-qubit IBM_LAGOS processor is shown in Fig. 2. This superconducting device can apply z rotations, X and $\sqrt{X}$ gates, reset operations and CNOT gates between connected qubits. These gates are implemented as microwave pulses that rotate the qubits in the Bloch sphere. The properties of the qubits, gates, and connections of the processor are provided in the Appendix. Each qubit is initially prepared in the $|0\rangle$ state, and by measuring it one has its projection on the computational basis. Thus, a quantum circuit must be executed several times in order to build a statistics of the measurements, each repetition called a shot. The number of shots can be defined by the user.

When mapping a quantum circuit to an IBM quantum processor, any gate that is not in this set must be expressed in terms of the available operations. Also, the connectivity of the topology must be considered since applying CNOT gates to unconnected qubits requires SWAP operations, which are expensive to perform on a noisy quantum device. All these steps may be performed automatically with QISKIT by a process called *transpilation* [44,45]. Besides rewriting a quantum circuit to match the topology of the real device, the transpilation also optimizes it for execution on noisy systems. In our problem, the interactions are all between neighboring qubits, thus, a good choice of layout is that shown in Fig. 2.
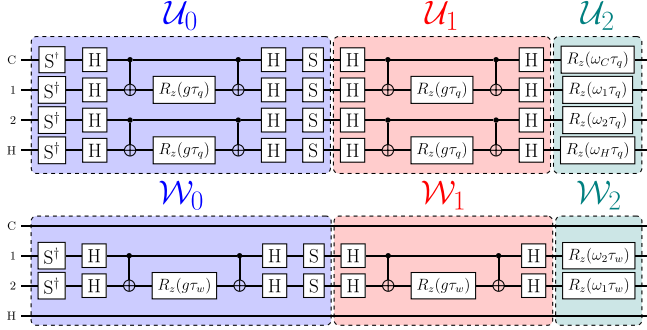
FIG. 3. Quantum circuits for the implementation of the heat (above) and work (below) strokes. S and H represent phase and Hadamard gates, respectively, and $R_z(\theta)$ are rotations of an angle θ around the z axis. Here $\mathcal{U}_0 = e^{-ig\tau_q(\sigma_y^C \sigma_y^1 + \sigma_y^2 \sigma_y^H)/2}$, $\mathcal{U}_1 = e^{-igt_q(\sigma_x^C \sigma_x^1 + \sigma_x^2 \sigma_x^H)/2}$, and $\mathcal{U}_2 = \prod_s e^{-igt_q(\omega_s \sigma_z^s)/2}$ for the heat stroke; $\mathcal{W}_0 = e^{-igt_w \sigma_y^1 \sigma_y^2/2}$, $\mathcal{W}_1 = e^{-igt_w \sigma_x^1 \sigma_x^2/2}$, and $\mathcal{W}_2 = e^{-igt_w(\omega_1 \sigma_z^1 + \omega_2 \sigma_z^2)/2}$ for the work stroke.

C. Quantum simulation

The dynamics of the system is implemented via quantum simulation, a process which consists of reproducing the dynamics of a quantum system using another quantum system [46]. For a system in an initial state $|\psi(0)\rangle$ under the action of a time-independent Hamiltonian H_S, the time evolution is given by the solution of the Schrödinger equation,

$$|\psi(t)\rangle = e^{-iH_S t/\hbar}|\psi(0)\rangle. \tag{19}$$

The problem consists of simulating the dynamics of H_S given by (19), using operations that can be implemented in the physical system that will act as the quantum simulator.

The evolution operators U_q and U_w for the heat and work strokes may be conveniently written as

$$U_q = e^{-ig(\sigma_y^C \sigma_y^1 + \sigma_y^2 \sigma_y^H)\tau_q/2} e^{-ig(\sigma_x^C \sigma_x^1 + \sigma_x^2 \sigma_x^H)\tau_q/2}$$
$$\times e^{-i(\omega_1 \sigma_z^1 + \omega_2 \sigma_z^2 + \omega_C \sigma_z^C + \omega_H \sigma_z^H)\tau_q/2}, \tag{20}$$

$$U_w = e^{-ig(\sigma_y^C \sigma_y^1 + \sigma_y^2 \sigma_y^H)\tau_w/2} e^{-ig(\sigma_x^C \sigma_x^1 + \sigma_x^2 \sigma_x^H)\tau_w/2}$$
$$\times e^{-i(\omega_1 \sigma_z^1 + \omega_2 \sigma_z^2)\tau_w/2}. \tag{21}$$

Thus, one must find a set of single- and two-qubit quantum gates $\mathcal{U}_m$ and $\mathcal{W}_m$ such that

$$U_q \approx \prod_{m=0}^{M} \mathcal{U}_m, \quad U_w \approx \prod_{m=0}^{M} \mathcal{W}_m. \tag{22}$$

Such a set can be found using the *Operator flow* module from QISKIT, and the resulting quantum circuits are shown in Fig. 3 with the parts that simulate each factor of Eqs. (20) and (21) being identified in the picture. The energy gaps of the qubits ω_x, $x = \{1, 2, C, H\}$, the coupling constant g, and the duration of each stroke are encoded in the angles of the rotations in both circuits, thus, one can change the system parameters in the quantum simulation by controlling these rotations.

D. Variational quantum thermalizer

At the beginning of each cycle the thermal states of the baths are prepared using a quantum circuit found with the VQT, which belongs to a class of variational algorithms called quantum-Hamiltonian-based models. Given a Hamiltonian H and a target inverse temperature $\beta = 1/T$, the goal of the VQT is to generate an approximation to the thermal state,

$$\rho_\beta = \frac{1}{\mathcal{Z}_\beta} e^{-\beta H}, \quad \mathcal{Z}_\beta = \text{Tr}\,(e^{-\beta H}), \tag{23}$$

where $\mathcal{Z}_\beta$ is the partition function.

We begin with a density matrix ρ_θ, defined by a set of pure states $\{|\psi_i\rangle\}$, that constitutes a basis on a Hilbert space of dimension d, and a parameter vector $\boldsymbol{\theta}$. Being $\{p_i(\theta_i)\}$ the probability distribution corresponding to the ith basis state, such a matrix can be written as

$$\rho_\theta = \sum_{i=1}^{d} p_i(\theta_i)|\psi_i\rangle\langle\psi_i|. \tag{24}$$

We sample from this distribution a pure state $|\psi_i\rangle$, pass it through a parametrized quantum circuit $U(\boldsymbol{\phi})$, and measure the mean energy $\langle H \rangle_i = \langle U(\boldsymbol{\phi})HU^\dagger(\boldsymbol{\phi})\rangle_{\psi_i}$. Repeating this process many times for the set $\{|\psi_i\rangle, p_i(\theta_i)\}$ and averaging the obtained $\langle H \rangle_i$ will give us the mean energy $\langle H \rangle_{\theta\phi}$ with respect to $\rho_{\theta\phi} = U(\boldsymbol{\phi})\rho_\theta U^\dagger(\boldsymbol{\phi})$,

$$\langle H \rangle_{\theta\phi} = \sum_{i=1}^{d} p_i(\theta_i)\langle H \rangle_i. \tag{25}$$

As in any variational algorithm, in order to find the optimal parameters $\{\boldsymbol{\theta}', \boldsymbol{\phi}'\}$ that solve the problem, we must find the minimum of a *loss function*, which here can be obtained from (25) and the von Neumann entropy $S(\rho_\theta) = -\text{Tr}\{\rho_\theta \ln(\rho_\theta)\}$,

$$\mathcal{L}(\boldsymbol{\theta}, \boldsymbol{\phi}) = \beta \langle H \rangle_{\theta\phi} - S(\rho_\theta), \tag{26}$$
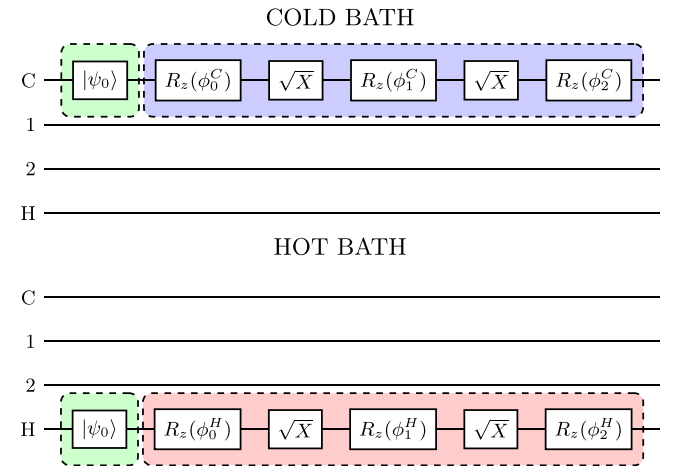

FIG. 4. The chosen ansatz for both thermal states consists of three R_z rotations interspersed by square root of NOT gates. Each rotation has a different ϕ parameter, which are to be optimized during the VQT implementation. The $|\psi_0\rangle$ gate sets the initial state to $|0\rangle$ or $|1\rangle$.
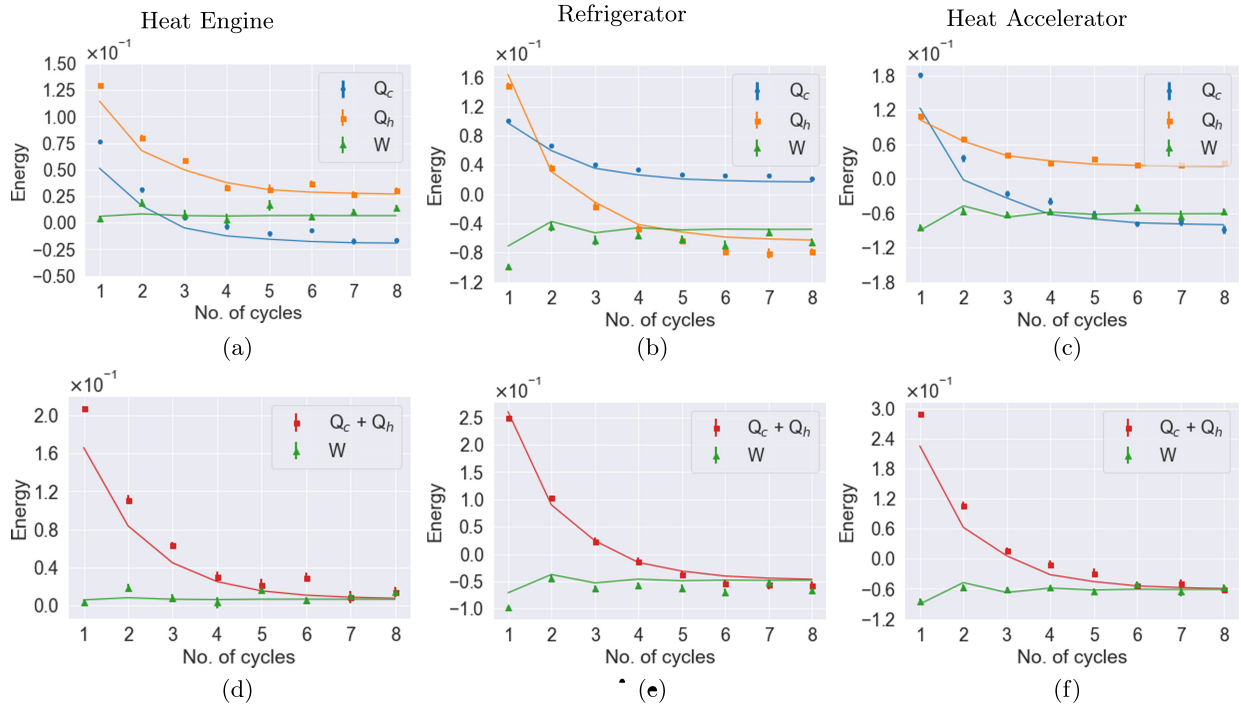
FIG. 5. Results for the three different modes of operation. First column: heat engine ($\omega_1 = 0.75$, $\omega_2 = 1.0$, $g = 0.80$, $T_C = 0.40$, and $T_H = 0.80$), second column: refrigerator ($\omega_1 = 0.50$, $\omega_2 = 2.0$, $g = 0.80$, $T_C = 1.0$, and $T_H = 1.2$), third column: heat accelerator ($\omega_1 = 2.0$, $\omega_2 = 0.50$, $g = 0.80$, $T_C = 1.0$, and $T_H = 1.2$). In all cases, both chain qubits were initialized in the ground state. Graphics (a)–(c) depict the dynamics of Q_C, Q_H, and W during the machine operation; graphics (d)–(f) are a statement of the first law, showing that $Q_C + Q_H$ and W converge to the same value in the limit cycle. The circles, squares, and triangles represent data from the quantum computer, and the solid lines are from a numerical simulation of the Trotter evolution. All results were obtained with 8192 shots (repetitions of the same circuit in order to build a statistics from the counts of $|0\rangle$ and $|1\rangle$). Each demonstration was repeated ten times, and the plot points represent the mean of the results of the expectation values. The error bars were calculated from three times the standard deviation.

which is minimized when $\rho_{\boldsymbol{\theta\phi}}$ is equal to the required thermal state with $\beta = 1/T$. This way, in order to control the temperature with the VQT, one must set the required temperature in the loss function. In order to calculate Eq. (26), the measurements of two quantities would be required, but we can take advantage from the fact that the entropy is invariant under unitary transformations on the density matrix: This way, only the energy measurement is necessary as the entropy can be calculated from the probability distribution parameters $\{\boldsymbol{\theta}\}$.

In our case, the baths have different temperatures T_C and T_H, so their thermal state preparation circuits must be found separately with VQT. As they are represented by a single qubit each ($d = 2$), one parameter θ is necessary to describe them, as $\rho_\theta = p(\theta)|0\rangle\langle 0| + [1 - p(\theta)]|1\rangle\langle 1|$, and their parametrized circuits must be executed two times in order to obtain the energy (25). The distribution $p(\theta)$ was chosen to be the sigmoid function $p(\theta) = 1/(1 + e^{-\theta})$. The ansatzes for the cold and hot baths are shown in Fig. 4. Their choice is based on the fact that they can approximate any one-qubit unitary [47], and take into account the set of gates accessible in IBM_LAGOS backend as discussed in Sec. III B. Other configurations were also tried, including rotations around other axes, but they did not show optimal results, and some demanded too many iterations of the VQT to converge. Therefore, the loss function $\mathcal{L}(\boldsymbol{\theta}, \boldsymbol{\phi})$ will contain four parameters to be classically optimized. The result of the VQT for both baths is a factorized state composed of

their two subsystems with dimension $d = 4$,

$$\rho_{CH} = \frac{1}{\mathcal{Z}_{\beta_C}} e^{-\beta_C H_C} \otimes \frac{1}{\mathcal{Z}_{\beta_H}} e^{-\beta_H H_H}, \qquad (27)$$

Thus, the whole procedure must be repeated four times, one for each element of the basis $\{|0\rangle, |1\rangle\} \otimes \{|0\rangle, |1\rangle\}$ as we are dealing with mixed states and IBMQ quantum circuits always start with pure states.

In order to implement the VQT, the open-source PYTHON library PENNYLANE [48] was used along with QISKIT. The classical optimization was performed using the SCIPY library [49] with the *constrained optimization BY linear approximation* method [50,51], which converged faster than other classical optimizers for our case. In general, it took less than 15 iterations for the algorithm to converge. When running the VQT on a quantum computer, it is important that it is performed in the corresponding qubits that will be used as thermal baths as in this case it finds optimal parameters that consider the device noise associated with those qubits during the learning process.

IV. RESULTS

The demonstrations were carried out for three different modes of operation of the machine: heat engine, refrigerator, and heat accelerator. They are determined by the values of the frequencies ω_1 and ω_2, and the temperatures T_C and T_H

TABLE I. Decoherence times, frequencies, and errors for the qubits.

Qubit	T_1 (us)	T_2 (us)	Frequencies (GHz)	Measured errors	Gate errors
C	142.53	101.29	5.188	6.000×10^{-3}	1.866×10^{-4}
1	139.32	129.54	5.100	6.900×10^{-3}	2.270×10^{-4}
2	143.70	127.84	4.987	1.850×10^{-2}	1.238×10^{-4}
H	149.91	106.99	5.176	1.500×10^{-2}	4.118×10^{-4}

TABLE II. Length and associated errors for the connections.

CNOT	Length (ns)	Error
C-1	327.11	5.930×10^{-3}
1-2	334.22	5.081×10^{-3}
2-H	334.22	1.053×10^{-2}

of the baths [39,42]. These modes can be observed when the machine reaches the limit cycle. In the interval $T_C/T_H \leqslant \omega_1/\omega_2 \leqslant 1$, it operates as a heat engine, withdrawing heat from the hot bath ($Q_H > 0$), expelling some of it in the cold bath ($Q_C < 0$) and producing some useful work ($W > 0$). When $\omega_1/\omega_2 < T_C/T_H$, it works as a refrigerator, consuming work ($W < 0$) in order to extract heat from the cold bath and transfer it to the hot bath ($Q_C > 0$, $Q_H < 0$). When $\omega_1/\omega_2 > 1$, the machine operates as a heat accelerator as it consumes work ($W < 0$) to accelerate the process of transferring heat from the hot to the cold bath ($Q_H > 0$, $Q_C < 0$).

The results are shown in Fig. 5. The columns contain the results for each mode of operation. For comparison purposes, a numerical simulation of the Trotter evolution was performed, represented by the solid lines in the graphics. Graphics (a)–(c) show the dynamics of the energetic flux during the cycles. As expected, the heat engine (a) and accelerator (c) show positive Q_H and negative Q_C in the limit cycle, whereas the refrigerator (b) presents the opposite behavior. During the work stroke, in the limit cycle, the heat engine produced work as denoted by $W > 0$, and the refrigerator and heat accelerator both consumed work in order to operate as denoted by $W < 0$. Graphics (d)–(f) show that the system obeys the first law as stated in Eq. (13): In the limit cycle, the sum of the heats $Q_C + Q_H$ and the work W converge to the same quantity.

V. CONCLUSIONS

To summarize, we demonstrated the use of the IBMQ processor as a tool to implement quantum heat engines with full access to the energetics of the system. Thermal reservoirs are, particularly, difficult to implement, which we overcame using a variational algorithm at each cycle, effectively implementing a collisional model. This allowed us to access both the limit cycle as well as the transient regime, offering unique insights into the relaxation process. Our approach cleanly separates the heat and work strokes, and, thus, can be readily generalized to any other type of heat engines. This means either chains with multiple qubits, or more complicated interactions, opening up the prospect of simulating quantum heat engines and quantum

transport in various many-body systems. Finally, although quantum coherence can emerge due to the interacting nature of the Hamiltonians of both strokes, it did not play a particular role in our study of the system dynamics. All coherence that arises between the baths and the system during the heat stroke is lost after the bath qubits are reset. However, a study in this direction, as discussed in Refs. [52,53], can be implemented within our framework as the IBMQ provides tools to perform measurements of quantum coherence and entanglement [54].

APPENDIX: SYSTEM PROPERTIES

Table I shows properties of the qubits used in the IBM_LAGOS processor. Average single-qubit gate length is of 35.56 ns. The readout length for all qubits is of 704.0 ns, and its associated error is 0.01. Table II shows the length of the CNOT gates and their respective errors for all the connections used in the quantum simulation. Further information about this and other processors can be found in Ref. [33] in the *Services* section.

[1] A. Auffèves, PRX Quantum **3**, 020101 (2022).

[2] B. Bertini, F. Heidrich-Meisner, C. Karrasch, T. Prosen, R. Steinigeweg, and M. Žnidarič, Rev. Mod. Phys. **93**, 025003 (2021).

[3] G. T. Landi, D. Poletti, and G. Schaller, arXiv:2104.14350

[4] J. J. Mendoza-Arenas, T. Grujic, D. Jaksch, and S. R. Clark, Phys. Rev. B **87**, 235130 (2013).

[5] V. Balachandran, G. Benenti, E. Pereira, G. Casati, and D. Poletti, Phys. Rev. Lett. **120**, 200603 (2018).

[6] C. Jarzynski, Phys. Rev. X **7**, 011008 (2017).

 [7] M. Perarnau-Llobet, H. Wilming, A. Riera, R. Gallego, and J. Eisert, Phys. Rev. Lett. **120**, 120602 (2018).

 [8] P. Strasberg, Phys. Rev. Lett. **123**, 180604 (2019).

 [9] P. Talkner and P. Hänggi, Rev. Mod. Phys. **92**, 041002 (2020).

[10] M. H. Partovi, Phys. Rev. E **77**, 021110 (2008).

[11] D. Jennings and T. Rudolph, Phys. Rev. E **81**, 061130 (2010).

[12] K. Micadei, J. P. S. Peterson, A. M. Souza, R. S. Sarthour, I. S. Oliveira, G. T. Landi, T. B. Batalhão, R. M. Serra, and E. Lutz, Nat. Commun. **10**, 2456 (2019).

[13] M. Perarnau-Llobet, E. Bäumer, K. V. Hovhannisyan, M. Huber, and A. Acin, Phys. Rev. Lett. **118**, 070601 (2017).

[14] K. Micadei, G. T. Landi, and E. Lutz, Phys. Rev. Lett. **124**, 090602 (2020).

[15] A. Levy and M. Lostaglio, PRX Quantum **1**, 010309 (2020).

[16] K. Micadei, J. P. S. Peterson, A. M. Souza, R. S. Sarthour, I. S. Oliveira, G. T. Landi, R. M. Serra, and E. Lutz, Phys. Rev. Lett. **127**, 180603 (2021).

[17] R. Kosloff and A. Levy, Annu. Rev. Phys. Chem. **65**, 365 (2014).

[18] M. T. Mitchison, Contemp. Phys. **60**, 164 (2019).

[19] J. Roßnagel, S. T. Dawkins, K. N. Tolazzi, O. Abah, E. Lutz, F. Schmidt-Kaler, and K. Singer, Science **352**, 325 (2016).

[20] D. von Lindenfels, O. Gräb, C. T. Schmiegelow, V. Kaushal, J. Schulz, M. T. Mitchison, J. Goold, F. Schmidt-Kaler, and U. G. Poschinger, Phys. Rev. Lett. **123**, 080602 (2019).

[21] G. Maslennikov, S. Ding, R. Hablützel, J. Gan, A. Roulet, S. Nimmrichter, J. Dai, V. Scarani, and D. Matsukevich, Nat. Commun. **10**, 202 (2019).

[22] N. V. Horne, D. Yum, T. Dutta, P. Hänggi, J. Gong, D. Poletti, and M. Mukherjee, npj Quantum Inf. **6**, 37 (2020).

[23] J. V. Koski, V. F. Maisi, J. P. Pekola, and D. V. Averin, Proc. Natl. Acad. Sci. USA **111**, 13786 (2014).

[24] J. V. Koski, A. Kutvonen, I. M. Khaymovich, T. Ala-Nissila, and J. P. Pekola, Phys. Rev. Lett. **115**, 260602 (2015).

[25] A. Solfanelli, A. Santini, and M. Campisi, PRX Quantum **2**, 030353 (2021).

[26] A. Solfanelli, A. Santini, and M. Campisi, AVS Quantum Sci. **4**, 026802 (2022).

[27] J. P. S. Peterson, T. B. Batalhão, M. Herrera, A. M. Souza, R. S. Sarthour, I. S. Oliveira, and R. M. Serra, Phys. Rev. Lett. **123**, 240601 (2019).

[28] T. Denzler, J. F. G. Santos, E. Lutz, and R. Serra, arXiv:2104.13427.

[29] K. Ono, S. N. Shevchenko, T. Mori, S. Moriyama, and F. Nori, Phys. Rev. Lett. **125**, 166802 (2020).

[30] Y. Zou, Y. Jiang, Y. Mei, X. Guo, and S. Du, Phys. Rev. Lett. **119**, 050602 (2017).

[31] J. Klatzow, J. N. Becker, P. M. Ledingham, C. Weinzetl, K. T. Kaczmarek, D. J. Saunders, J. Nunn, I. A. Walmsley, R. Uzdin, and E. Poem, Phys. Rev. Lett. **122**, 110601 (2019).

[32] W. Ji, Z. Chai, M. Wang, Y. Guo, X. Rong, F. Shi, C. Ren, Y. Wang, and J. Du, Phys. Rev. Lett. **128**, 090602 (2022).

[33] IBM Quantum, https://quantum-computing.ibm.com/

[34] V. Scarani, M. Ziman, P. Štelmachovič, N. Gisin, and V. Bužek, Phys. Rev. Lett. **88**, 097905 (2002).

[35] H. T. Quan, Y.-x. Liu, C. P. Sun, and F. Nori, Phys. Rev. E **76**, 031105 (2007).

[36] A. E. Allahverdyan, K. Hovhannisyan, and G. Mahler, Phys. Rev. E **81**, 051129 (2010).

[37] R. Uzdin and R. Kosloff, New J. Phys. **16**, 095003 (2014).

[38] M. Campisi, J. Phys. A: Math. Theor. **47**, 245001 (2014).

[39] M. Campisi, J. Pekola, and R. Fazio, New J. Phys. **17**, 035012 (2015).

[40] O. A. D. Molitor and G. T. Landi, Phys. Rev. A **102**, 042217 (2020).

[41] G. Verdon, J. Marks, S. Nanda, S. Leichenauer, and J. Hidary, arXiv:1910.02071.

[42] G. De Chiara, G. Landi, A. Hewgill, B. Reid, A. Ferraro, A. J. Roncaglia, and M. Antezza, New J. Phys. **20**, 113024 (2018).

[43] P. Krantz, M. Kjaergaard, F. Yan, T. P. Orlando, S. Gustavsson, and W. D. Oliver, Appl. Phys. Rev. **6**, 021318 (2019).

[44] G. Aleksandrowicz, T. Alexander, P. Barkoutsos, L. Bello, Y. Ben-Haim, D. Bucher, F. J. Cabrera-Hernández, J. Carballo-Franquis, A. Chen, C.-F. Chen, J. M. Chow, A. D. Córcoles-Gonzales, A. J. Cross, A. Cross, J. Cruz-Benito, C. Culver, S. D. L. P. González, E. D. L. Torre, D. Ding, E. Dumitrescu *et al.*, Qiskit: An Open-source Framework for Quantum Computing (2019).

[45] M. Treinish, I. Carvalho, G. Tsilimigkounakis, and N. Sá, arXiv:2110.15221 (2021).

[46] R. P. Feynman, Int. J. Theor. Phys. **21**, 467 (1982).

[47] M. A. Nielsen and I. Chuang, *Quantum Computation and Quantum Information* (American Association of Physics Teachers, College Park, MD, 2002).

[48] V. Bergholm, J. Izaac, M. Schuld, C. Gogolin, S. Ahmed, V. Ajith, M. S. Alam, G. Alonso-Linaje, B. AkashNarayanan, A. Asadi, J. M. Arrazola, U. Azad, S. Banning, C. Blank, T. R Bromley, B. A. Cordier, J. Ceroni, A. Delgado, O. Di Matteo, A. Dusko *et al.*, arXiv:1811.04968.

[49] P. Virtanen, R. Gommers, T. E. Oliphant, M. Haberland, T. Reddy, D. Cournapeau, E. Burovski, P. Peterson, W. Weckesser, J. Bright, S. J. van der Walt, M. Brett, J. Wilson, K. J. Millman, N. Mayorov, A. R. J. Nelson, E. Jones, R. Kern, E. Larson, C. J. Carey *et al.*, Nat. Methods **17**, 261 (2020).

[50] M. J. Powell, *Advances in Optimization and Numerical Analysis* (Springer, Dordrecht, 1994), pp. 51–67.

[51] M. J. Powell, Acta Numer. **7**, 287 (1998).

[52] K. Korzekwa, M. Lostaglio, J. Oppenheim, and D. Jennings, New J. Phys. **18**, 023045 (2016).

[53] B. d. L. Bernardo, Phys. Rev. E **102**, 062152 (2020).

[54] R. Horodecki, P. Horodecki, M. Horodecki, and K. Horodecki, Rev. Mod. Phys. **81**, 865 (2009).

[55] J. Johansson, P. Nation, and F. Nori, Comput. Phys. Commun. **184**, 1234 (2013).

[56] A. Kay, QUANTIKZ (2019).

[57] https://github.com/lipinor/two-stroke-qhe-vqt